Electrical Power and Energy Systems 156 (2024) 109782

Contents lists available at ScienceDirect

International Journal of Electrical Power and Energy Systems

journal homepage: www.elsevier.com/locate/ijepes

Power quality of DC microgrid: Index classification, definition, correlation analysis and cases study

Jianquan Liao [a], Yangtao Liu [a], Chunsheng Guo [a], Niancheng Zhou [b], Qianggang Wang [b], Wenfa Kang [b,*], Juan C. Vasquez [c], Josep M. Guerrero [d]

[a] Sichuan University, School of Electrical Engineering, Chengdu, China
[b] Chongqing University, School of Electrical Engineering, Chongqing, China
[c] AAU Energy, Aalborg University, Denmark
[d] Center for Research on Microgrids, Technical University of Catalonia, Spanish

ARTICLE INFO

Keywords:
DC microgrid
Power quality
Index definition
Correlation analysis

ABSTRACT

DC microgrid has a promising future for its strong power supply capacity, good controllability, and high efficiency. The power quality of the DC microgrid is one of the core issues of planning, design, operation, and control. However, due to the zero-frequency characteristic of DC system, its power quality presents new characteristics. This paper analyzes the differences between AC and DC power quality and constructs the DC power quality index system. The DC harmonic, voltage fluctuation and flicker, voltage sag, voltage unbalances, and voltage deviations are defined according to the existing literature and standards. Moreover, the correlation between harmonics and fluctuations, voltage deviations and steady-state unbalances, voltage sags and transient unbalances are analyzed. Subsequently, the typical cases of the DC microgrids are selected to analyze the generation mechanism of each power quality phenomenon under different working conditions. According to the proposed index definition, the quantitative relationship between the indexes and the related parameters is obtained. The simulation cases are built to verify the generation mechanism and index relevance.

1. Introduction

The interconnection and regulation of power supply, load, and energy storage of DC microgrids are realized in the DC form through power electronic technology [1]. DC microgrid has the advantages of large power supply capacity, high reliability, and strong "source to load adaptability", which has become a research hotspot worldwide [1–3]. The promotion of DC microgrid requires deepening the top-level design of voltage-level sequence and typical topological structure, breaking through basic research such as planning, design and operation control, protection, and key technologies such as DC transformers and circuit breakers [2,3]. DC power quality is one of the keys in DC microgrid planning, design, and operation control that will directly affect the application and development of DC microgrid technology.

According to the generation mechanism of power quality in the DC microgrid, the DC power quality phenomenon can be divided into two categories: steady-state and transient state. The steady-state phenomenon refers to the continuous power quality disturbance caused by the fluctuation of load and renewable energy [3]. The transient phenomenon refers to the short-term power quality disturbances and electromagnetic transient phenomena caused by interference of power network faults, switching operation, and active control [4].

In terms of the steady-state power quality phenomenon, [5] analyzes the ripple formation mechanism and superposition characteristics on the DC side of the DC microgrid. The calculation method of unbalanced voltage in bipolar DC microgrid is given in [6]. [3] discusses the generation mechanism of bus voltage fluctuation in the DC microgrid. A method for calculating the DC side harmonic current of a hybrid HVDC transmission system is proposed in [7], and a filter is designed to suppress the DC side low-frequency voltage ripple. In terms of the transient power quality phenomenon, it is pointed out that 65 % of the power quality problems in the network are caused by voltage sag [8]. In [9], the impacts of different grounding faults on the voltage balance of the DC microgrid are analyzed. [10] points out that voltage sag is usually caused by short circuit fault in the power grid, which is considered as one of the main power quality problems. The influence of voltage sags caused by balanced faults and unbalanced faults are discussed in [11].

It can be concluded that the DC power quality phenomenon has attracted extensive attention from scholars. However, as the DC power

* Corresponding author.
E-mail address: kwf.ac@outlook.com (W. Kang).

https://doi.org/10.1016/j.ijepes.2024.109782
Received 6 January 2023; Received in revised form 12 October 2023; Accepted 3 January 2024
Available online 9 January 2024

Nomenclature

A	voltage or current of DC bus
HRA_h	h^{th} harmonic content ratio
A_H	harmonic content
$THDA$	total harmonic distortion rate
A_h	RMS value of the h^{th} harmonic
A_d	RMS value of DC bus voltage or current
T_s	the sampling period
u_p, u_g	the peak and valley values in a sampling period
U_{dN}	nominal DC bus voltage
δ%	voltage fluctuations coefficient
Mod%	DC voltage flicker depth
FI%	flicker percentage
ϕ_{max}, ϕ_{avg}, ϕ_{min}	maximum, average, and minimum luminous flux values
S_1, S_2	areas above and below ϕ_{avg}
ε_u%	voltage unbalance coefficient
V_+, V_-	RMS values of positive and negative DC bus voltage
ΔU%	voltage deviation percentage
U_i	the actual measured voltage if i^{th} node
ΔV_{sag}%	DC voltage sag depth
u_d, u'_d	the actual measured values of the DC voltage before and after the sag
f_1, f_c	fundamental frequency, carrier frequency
m	the number of harmonics in the carrier frequency band
n	the number of harmonics in the m^{th} carrier frequency band
U_{Nm}	the nominal voltage of the AC side
U_c	the amplitude of the carrier voltage
M	the amplitude modulation ratio
S_a, S_b, S_c	Switching function of VSC
I_{m1}, I_{m2}, I_{m0}	the amplitudes of the positive, negative and zero sequence components
φ_1, φ_2, φ_0	the amplitudes of the positive, negative and zero sequence current phases
i_{dc}	DC side current
u	Instantaneous DC voltage
U_{d0}	DC component of DC bus voltage
U_1 to U_n	RMS value of 1st to n^{th} voltage harmonic
φ_1 to φ_n	initial phase angle of 1st to n^{th} voltage harmonic
T_h	the transfer coefficient of h^{th} harmonic
Z_{Ch}	the characteristic impedance corresponding to the h^{th} harmonic
l	the length of DC line
γ_h	the propagation constant corresponding to h^{th} harmonic
z_{oh}, y_{oh}	the reactance and susceptance of the h^{th} harmonic
V_s	equivalent voltage of DC bus
R_L	equivalent resistance of positive, negative, and neutral line
R_p, R_n	equivalent resistance of positive and negative DC loads
P_p, P_n	equivalent power of positive and negative DC loads
C_{vuf}	Voltage unbalance correlation coefficient between node i and j
$C_{\Delta V+}$	Positive pole voltage deviation correlation coefficient between node i and j
$C_{\Delta V-}$	negative pole voltage deviation correlation coefficient between node i and j
T_h	the transfer coefficient of h^{th} harmonic
Z_{Ch}	the characteristic impedance corresponding to the h^{th} harmonic
l	the length of DC line
γ_h	the propagation constant corresponding to h^{th} harmonic
z_{oh}, y_{oh}	the reactance and susceptance of the h^{th} harmonic
V_s	equivalent voltage of DC bus
R_L	equivalent resistance of positive, negative, and neutral line
R_p, R_n	equivalent resistance of positive and negative DC loads
P_p, P_n	equivalent power of positive and negative DC loads
C_{vuf}	Voltage unbalance correlation coefficient between node i and j
$C_{\Delta V+}$	Positive pole voltage deviation correlation coefficient between node i and j
$C_{\Delta V-}$	negative pole voltage deviation correlation coefficient between node i and j
T_h	the transfer coefficient of h^{th} harmonic
Z_{Ch}	the characteristic impedance corresponding to the h^{th} harmonic
l	the length of DC line
γ_h	the propagation constant corresponding to h^{th} harmonic
z_{oh}, y_{oh}	the reactance and susceptance of the h^{th} harmonic
V_s	equivalent voltage of DC bus

quality index system has not been established, there are some problems in the above literature, such as inconsistent concepts and unclear definitions. For example, [5] divides the ripple on the DC side into 1st, 2nd, and k^{th} ripples according to the power frequency and its multiples. Besides, the expression of the ripple content and the total ripple distortion rate are defined. This is the same as the definition of DC harmonic in the IEEE DC transmission standard [12], but it does not explain the difference between DC ripple and DC harmonic. In [13–15], the suppression methods of the second harmonic current of the converter are proposed. However, the papers adopt the term "voltage/current ripple" for the description of DC harmonics and do not consider the relationship between ripple and harmonics. At the same time, [16] classifies the "DC ripple" caused by power grid harmonics and imbalance as oscillatory voltage fluctuation. [17,18] both use "ripple" to define the AC component in the DC bus voltage, while [19,20] define it as "harmonic". [21] proposes a harmonic suppression strategy for DC distribution systems based on hybrid DC electric spring (DC-ES). However, there is no clear definition of the ripple and harmonics mentioned in the article. It can be concluded that the definitions of harmonics, fluctuation, and ripple in the existing literature are inconsistent, and the correlation has not been investigated. The inconsistency of this definition makes it difficult to carry out standardized management of power quality or standardized production of electrical equipment.

The above references have different interpretations for the same phenomenon which also appears in the definition and correlation analysis of voltage deviation, voltage sag, and voltage unbalance. [22] studies the limitation of DC voltage deviation of DC microgrid but does not analyze the difference between voltage deviation and voltage sag. [23] mentions that when the DC load switching, the low-frequency flicker of the bus voltage will be caused in the DC grids. However, the mechanism of low-frequency voltage flicker has not been analyzed in depth, nor has it explained the difference between DC voltage flicker and AC voltage flicker. The method of stabilizing the DC voltage deviation and voltage unbalance coefficient is discussed in [24], and a voltage regulation strategy based on system impedance parameter identification is proposed. Furthermore, the correlation between voltage deviation and voltage unbalance coefficient is also considered. However, the DC voltage deviation and voltage unbalance coefficient are not defined as indicators, and the DC power quality system is not established in [24]. The unification of classification and definition of DC power quality phenomena is the basis for carrying out relevant work, which is of great significance for the popularization and application of DC microgrids.

To solve the above problems, this paper studies the definition and power quality index system of the DC microgrid. The contributions of

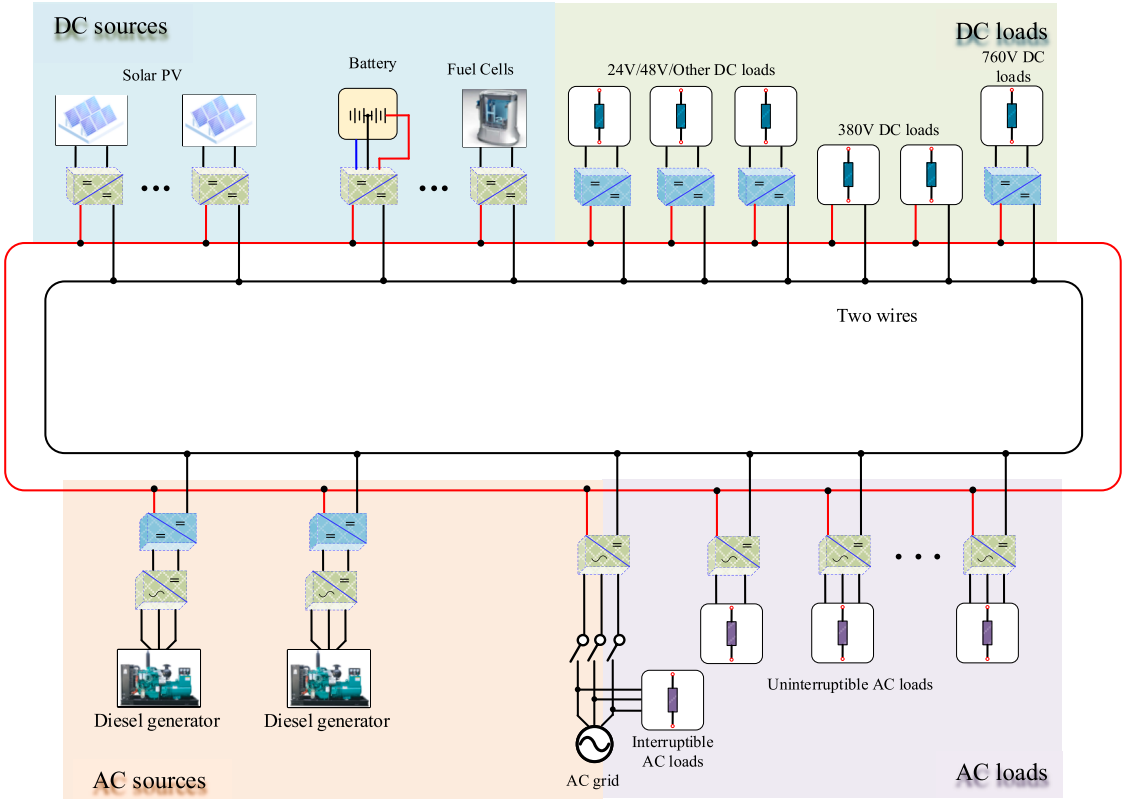

(a)

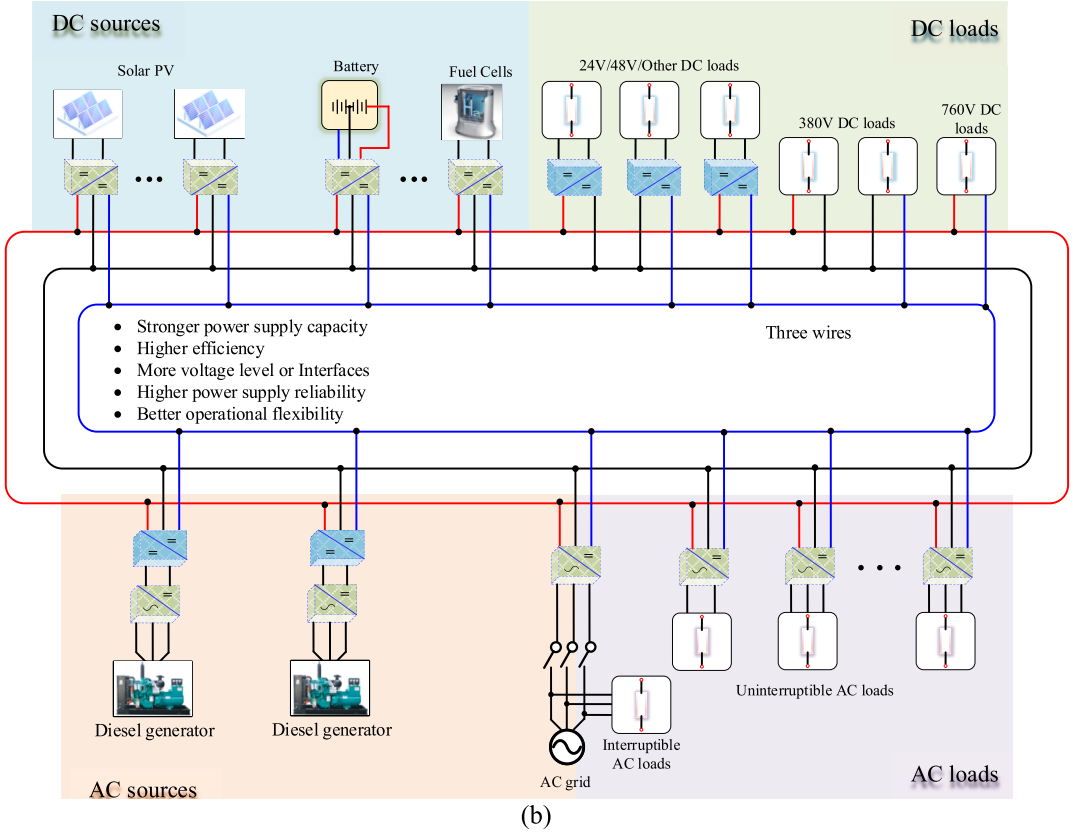

(b)

Fig. 1. Typical DC microgrid structure: (a) unipolar DC microgrid, (b) bipolar DC microgrid.

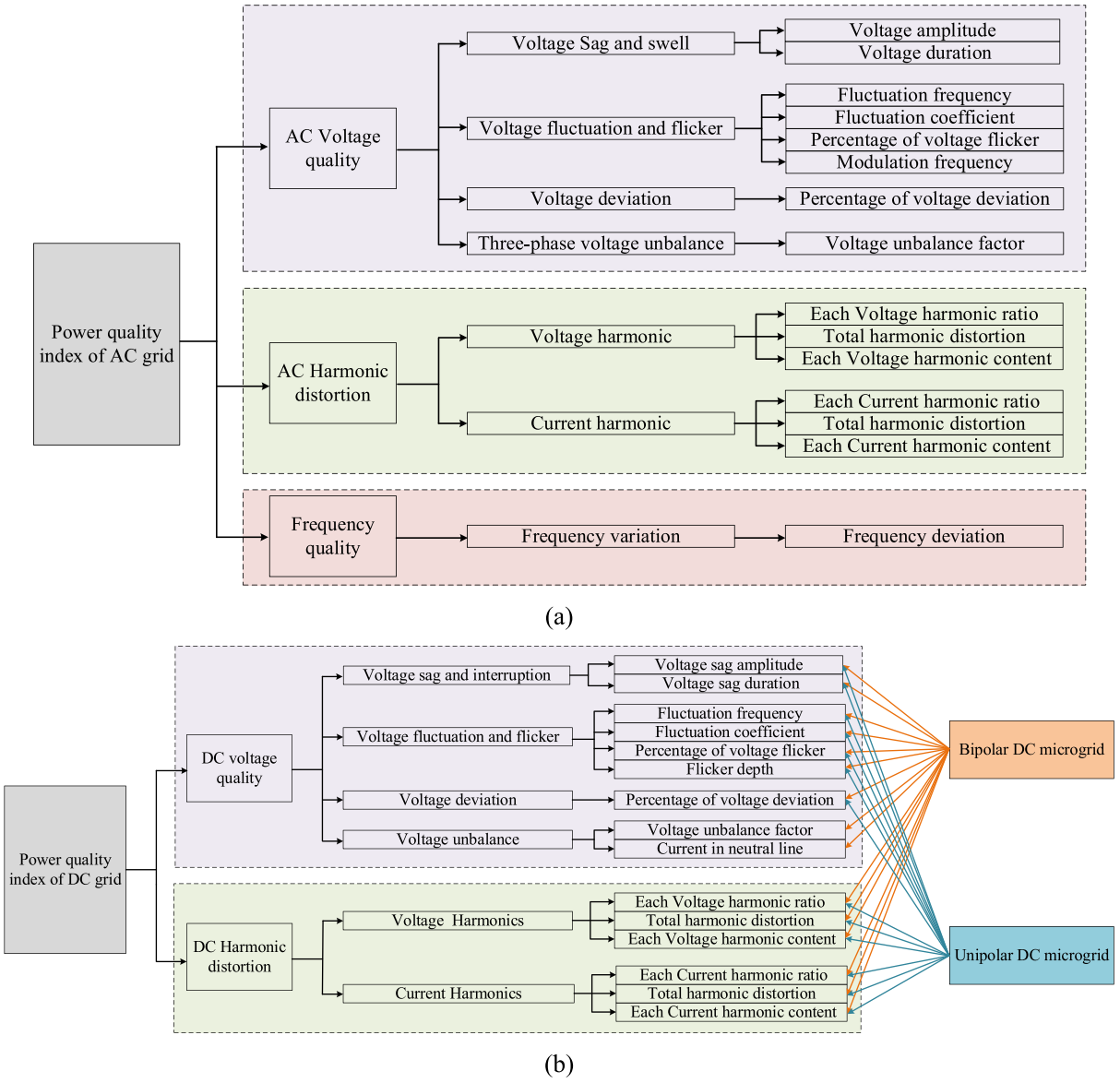

Fig. 2. Index system of AC and DC power quality: (a) AC microgrid, (b) DC microgrid.

this study are as follows:

1) The differences between AC and DC power quality phenomena are analyzed. On this basis, the different power quality phenomena are defined according to existing references or standards, and the DC power quality index system is established.
2) The correlation between different DC power quality phenomena is analyzed, and the importance of the DC power quality index system in measurement, standard valuation, and index limitation are elaborated.
3) The typical cases of DC microgrid are selected to analyze the generation mechanism of power quality phenomenon and the calculation method of indicators under different working conditions, and the correlation between indicators is verified through simulation cases.

The remaining structure of this paper is as follows. Section 1 presents the DC power quality and related analysis. Section 2 discusses DC voltage harmonics and fluctuations. In Section 3, DC voltage imbalance and DC voltage sag are analyzed. Section 4 shows the simulation and experimental results about power quality in the bipolar DC microgrid. Section 5 is the summary of this paper.

2. DC power quality index system and the correlation analysis

2.1. Power quality index system of DC microgrid

According to the DC bus frames, DC microgrid is classified into two categories: unipolar (two wires) and bipolar (three wires) DC bus design [25], as shown in Fig. 1(a and b), respectively. Unlike a unipolar DC microgrid, a bipolar structure adopts two different voltage levels. Utilizing a bipolar DC topology efficiently reduces power conversion while increasing overall efficiency [26]. To better utilize the DC power grid, the bipolar topology is possible to combine DGs, green buildings, and EVs more flexibly [27]. Like a three-phase AC system, a bipolar DC microgrid increases the system stability due to the separate operating of the two poles [28]. Furthermore, the other two lines can maintain the regular operation of the system even if one of the DC buses fails [29].

In general, the AC system is connected to the DC microgrid through an AC/DC converter. However, when the power supply inside the DC microgrid is sufficient, the AC system will be isolated so that the DC microgrid operates in an island mode. Therefore, DC microgrid will be

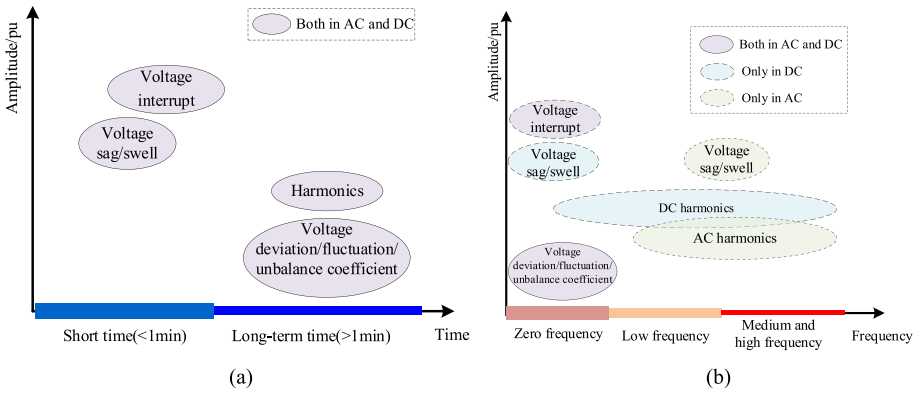

Fig. 3. Characteristics of AC/DC power quality:(a) Multi time scale distribution characteristics and (b) Broadband distribution characteristics.

connected to an AC system, DC system or just a stand-alone microgrid. In high-voltage level DC systems, the operating characteristics of the system are relatively stable, for example, the bipolar load is generally balanced. Therefore, the power quality problem of high voltage level scenarios is not much concerned. However, the indicators and correlations defined or analyzed in this study are independent of voltage levels.

Compared with the AC microgrid, the DC microgrid does not need to consider frequency and power-angle stability. Besides, the DC microgrid avoids the mutual coupling between active power and frequency, and reactive power and voltage in the AC system. Besides, the operation of DC microgrid can be realized by controlling DC bus voltage [23]. Therefore, the power quality of DC microgrid present new characteristics due to its zero-frequency characteristics, as shown below:

1) When the DC microgrid is connected to the AC system through an AC/DC converter, the disturbance of the AC system has a great impact on the power quality of the DC microgrid. For example, the fault of the AC system will cause a large fluctuation of DC bus voltage [9], the imbalance of AC voltage will cause a low-frequency harmonic of DC voltage through DC converter, and AC single-phase devices will introduce second harmonic components that superimpose on the DC component [30].
2) The power fluctuation of distributed generations (DGs) and DC loads (such as electric vehicles) lead to the voltage fluctuation of the DC microgrid being much higher than AC microgrid [9].
3) In addition, the response time of DC load to DC power quality disturbance is smaller than that of the AC microgrid. A small disturbance may cause sensitive DC loads unable to work normally, resulting in large economic losses.

At present, the research on DC power quality has not been fully investigated, and its definition and classification have not been unified. In addition, the relevant DC power quality standards have not been formed [31]. Therefore, it is necessary to refer to the power quality index system of the AC microgrid and consider the differences between AC and DC systems. Moreover, the phenomena of DC power quality need to be classified, defined, and established. Finally, a power quality index system of the DC microgrid should be built. The AC power quality index system is shown in Fig. 2(a) [32].

According to the existing literature, DC power quality phenomena include voltage fluctuation and flicker [33,34], voltage harmonics [19,20], voltage sag and short-term interruption [10], voltage imbalances [25], voltage deviation [22]. The voltage imbalance mentioned in this study is for the bipolar DC microgrid, which can be divided into transient imbalance and steady-state imbalance. Compared with the AC power quality index system, since the DC microgrid has no frequency and phase-angle problems, the DC power quality index system is divided into harmonic distortion and voltage quality. The specific indexes of each power quality phenomenon are given in [30,35], and the power quality index system of the DC microgrid is shown in Fig. 2(b).

2.2. Correlation analysis of power quality indexes in DC microgrid

Fig. 3 compares the multi-time scale and broadband distribution characteristics of AC and DC power quality events from the characteristic parameters of amplitude, frequency, and disturbance time. According to the characteristic parameters of power quality events in DC distribution networks, power quality problems can be divided into transient and steady state [36].

Transient events have the characteristics of large amplitude change and short-term disturbance, which are caused by power grid fault, switch operation and control system disturbance [37], such as voltage sag and voltage swell; Steady-state events have the characteristics of small amplitude change and continuous emission, which are caused by fluctuation of load, renewable energy and exchange power change of contact points in multi-level power grid [38], such as voltage imbalance, voltage deviation, voltage fluctuation and harmonics.

The power source, network, and load are the basic components of the DC microgrid. Their continuous emission and short-term disturbance will lead to corresponding steady-state and transient power quality

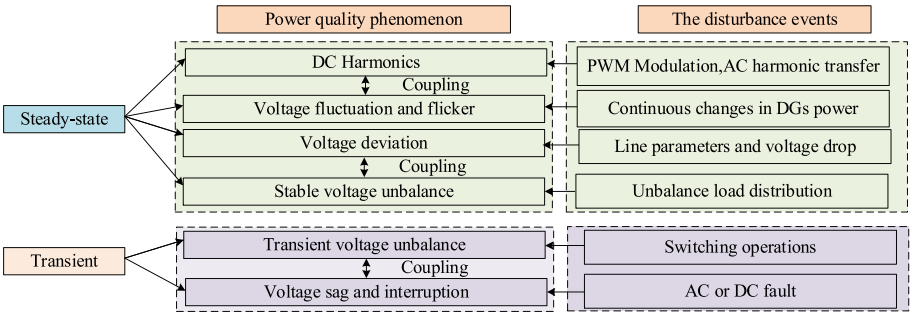

Fig. 4. Correlation of DC power quality indexes.

problems. DC voltage harmonics and fluctuations are caused by equipment attributes such as modulation characteristics of pulse width modulation (PWM) converter and line-commutation converter (LCC) [5]. Besides, the randomness and uncertainty of power consumption of DGs, and DC load will also lead to voltage fluctuations and harmonics.

Steady-state voltage imbalance is caused by unbalanced load distribution at two poles, and voltage deviation is caused by line voltage drop [22]. They can be classified as steady-state phenomena. The DC voltage sag [10] and transient voltage imbalance [9] caused by short-term disturbances such as DC faults, equipment switching, and external impact belong to transient phenomena. Due to the zero frequency characteristics of DC voltage and the structure of the DC microgrid, there are coupling characteristics between harmonics and fluctuations, and the coupling also exists in voltage deviation and steady-state voltage imbalance. In addition, there is also a coupling relationship between voltage sag and transient voltage imbalance under the same disturbance in the bipolar DC microgrid. The correlation between different power quality phenomena is shown in Fig. 4.

It can be seen from Fig. 4 the difference between AC and DC power quality phenomenon is prominent. Moreover, the correlation between the various indicators is significantly enhanced which reflects the difference. Therefore, the correlation analysis is the basis of understanding and solving the DC power quality problems.

1) When formulating the DC power quality standards, it is necessary to deal with specific application scenarios or voltage levels. According to the correlation between different indicators, the corresponding evaluation can be reduced to realize the consolidation and simplification of indicators. In a low-voltage DC microgrid, the ripple coefficient is adopted instead of the concept of harmonic to evaluate DC voltage fluctuation [39]. However, with the improvement of DC microgrid voltage level, the concept of ripple cannot fully describe DC power quality. For the medium voltage level in the DC microgrid, the application of a power quality index system including harmonics is consistent with the academic definition of the AC microgrid. This is not only conducive to the development of relevant work but also effective to the transfer of research results of AC power quality to DC power quality.
2) The correlation between various indexes of DC power quality is an important basis for formulating index limitations. For a specific application scenario, any power quality exceeding the standard may have an adverse impact on the normal operation of the system or DC load. Therefore, the formulation of the limit value shall meet the limitation range of the related indicators at the same time. For example, in a bipolar DC microgrid, if the voltage deviation of one pole is within the limitation, the voltage unbalance coefficient may exceed the standard and these two indicators are mutually restrictive [31].

3. Definition of DC power quality index

3.1. DC harmonics

The scholars still adopt the terms such as ripple [17,40], fluctuation [9,41], pulsation [7,42] to describe the AC components in DC voltage. DGs and loads in the DC microgrid are connected through power electronic devices, so the DC bus contains modulated harmonics [43,44]. In addition, the three-phase imbalance of AC voltage and single-phase AC loads will produce even-order harmonics and low-frequency harmonics on the DC side [20]. Consequently, DC harmonics exist in different frequency bands and have their own characteristics, so the concept of "harmonic" should be introduced to describe them.

In this paper, the periodic AC component superimposed in a constant DC voltage or current is defined as DC voltage harmonic or current harmonic. To measure the voltage or current harmonic content, HRA_h, A_H, and $THDA$ are defined [45], and the expressions are shown in Eq. (1).

$$\begin{cases} HRA_{\mathrm{dc}} = \dfrac{A_h}{A_{\mathrm{dc}}} \times 100\% \\ A_{\mathrm{H}} = \sqrt{\sum_{h=1}^{\infty} (A_h)^2} \\ THDA_{\mathrm{dc}} = \dfrac{A_{\mathrm{H}}}{A_{\mathrm{dc}}} \end{cases} \tag{1}$$

Where HRA_{dc} and $THDA_{\mathrm{dc}}$ represent DC harmonic distortion and DC total harmonic distortion (THD), respectively. A_{h} represents the amplitude of the harmonic component with a frequency of h and A_{dc} represents the amplitude of the DC component.

It's important to note the differences between AC and DC Harmonic distortion. AC harmonic distortion refers to the distortion that exists between the harmonic components, beyond the fundamental frequency, and the ideal sinusoidal waveform in AC current or voltage waveforms. This distortion is calculated using the formula presented in (2). Conversely, DC harmonic distortion pertains to the distortion between the harmonic components, beyond the DC component, and the ideal DC voltage or current waveform. The fundamental distinction between AC and DC Harmonic distortion lies in the reference quantity used for calculation. In AC Harmonic distortion, the reference amplitude is that of the fundamental frequency (e.g., 50 Hz or 60 Hz), while in DC Harmonic distortion, the reference amplitude is that of the DC component (0 Hz). This fundamental difference in the definition and respective calculation formulas of AC and DC harmonic distortion also leads to their total harmonic distortion (THD) calculations, as indicated in Eq. (2).

$$\begin{cases} HRA_{ac} = \dfrac{A_h}{A_{\mathrm{fun}}} \times 100\% \\ THDA_{\mathrm{ac}} = \sqrt{\dfrac{\sum_{h=1}^{\infty} (A_h)^2}{A_{\mathrm{ac}}^2}} \end{cases} \tag{2}$$

Harmonics can indeed have adverse effects on equipment performance, efficiency, and overall system stability in DC systems. These effects can be specified in the following ways:

- For energy storage batteries within a DC system, harmonics can lead to an increase in the peak-to-peak current flowing into the batteries. When this exceeds 8 % of the rated current, it not only reduces battery efficiency but also causes damage and shortens their lifespan [46].
- In DC systems with a significant presence of power electronic devices, harmonic can result in wasted converter capacity and impact the lifespan of power electronic components [47]. This phenomenon increases the current stress and conduction losses of switching devices, leading to decreased converter efficiency. If soft-switching techniques are employed in DC/DC converters, harmonics can further limit the soft-switching range, leading to increased switching losses and decreased conversion efficiency [48].
- Concerning photovoltaic (PV) power generation, harmonics affect the implementation of maximum power point tracking (MPPT), causing output power to oscillate around the maximum power point [49,50]. This, in turn, reduces the efficiency of solar energy utilization.
- For electric devices, harmonics can result in increased noise and vibration in electric motors, thereby reducing their efficiency and lifespan. Additionally, harmonics can lead to LED flicker [51].

These effects underscore the significance of addressing harmonic distortion in DC systems and emphasize the importance of comprehensive harmonic analysis and mitigation strategies in such systems.

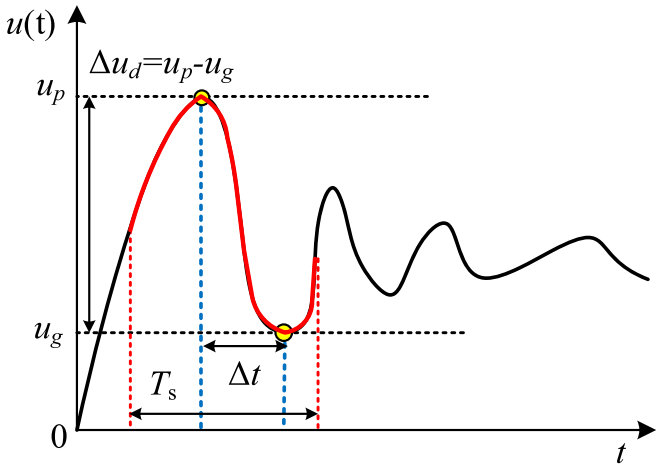

Fig. 5. DC bus voltage fluctuation diagram.

3.2. DC voltage fluctuation

The equivalent model of a DC power supply system is not an infinite power source, so the fast and continuous change of the source and load power in a DC microgrid will cause the fluctuation of DC voltage. It is a continuous change within a certain range of amplitude fluctuations under the premise of system stability. The DC voltage oscillation caused by the disturbance and resonance of the control system is different from the voltage fluctuation [52]. To evaluate the impact of voltage fluctuation on DC load, the index of DC bus voltage fluctuation needs to be further defined [53]. A DC voltage waveform is obtained by simulation as shown in Fig. 5. The derivative of this waveform is obtained to describe the number of voltage variations by obtaining positive and negative derivatives for each extreme point and for different intervals. As shown in Fig. 5, the DC bus voltage fluctuations can be assessed by the fluctuation frequency, the rate of voltage change, and the amplitude of fluctuations during the sampling period. Subsequently, the amplitude of voltage fluctuations coefficient can be further expressed as:

$$\delta\% = \frac{u_p - u_g}{U_{dN}} \times 100\% = \frac{\Delta u_d}{U_{dN}} \times 100\% \tag{3}$$

where U_{dN} is the rated voltage of the DC bus which is corresponding to the DC voltage level of the measuring point.

For illuminating equipment, in addition to (3) which can be used to assess the fluctuation of the DC bus voltage, an additional metric, namely flicker, can also be employed as an indicator for the evaluation of DC bus voltage fluctuations. The human visual response to unstable light illumination caused by voltage fluctuations is called flicker [27], which is similar to the flicker problem in AC power distribution. The flicker severity is related to the voltage fluctuation factor and the type of driving circuit. Due to the essential difference between AC and DC signals and the difference of LED drive transfer function, the flicker phenomenon in DC power quality needs further study. AC signal is related to flicker through inter harmonics, while low-frequency signal in DC bus is directly transmitted to LED which makes flicker more prominent. IEEE standard PAR1789 [54] recommends adopting flicker depth *Mod*% (also known as modulation depth) and flicker percentage *FI* (also known as modulation rate) to assess the severity of LED flicker. The relevant physical quantities are shown in Fig. 6. Fig. 6(a) shows the variation of LED luminous flux over a period. ϕ_{max}, ϕ_{avg} and ϕ_{min} is the maximum, average, and minimum luminous flux values, respectively. S_1 and S_2 are areas above and below ϕ_{avg}, respectively. Fig. 6(b) is the limitation range for *Mod*% for signals of different frequencies, which is classified as safe, low-risk, and not allowed. The physical meaning of *Mod*% is the ratio of ϕ_{max}-ϕ_{min} to $\phi_{max} + \phi_{min}$ during the sampling period. The *FI* is the percentage of the ratio of the area that exceeds the average luminous to the total area flux in the region.

$$Mod\% = \frac{\phi_{max} - \phi_{min}}{\phi_{max} + \phi_{min}} \times 100\% \tag{4}$$

$$FI\% = \frac{S_1}{S_1 + S_2} \times 100\% \tag{5}$$

3.3. Analysis of single-phase AC loads and DC voltage harmonics

For the incorporation of single-phase AC loads into the DC microgrid system, a schematic representation is depicted in Fig. 7. In this figure, v_o and i_o represent the voltage and current of the single-phase AC load,

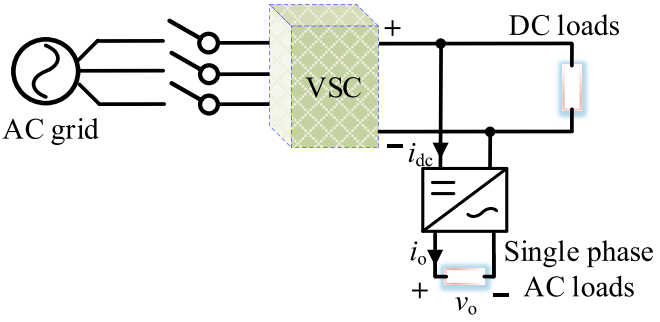

Fig. 7. Topology diagram for DC voltage harmonics analysis including single-phase AC loads.

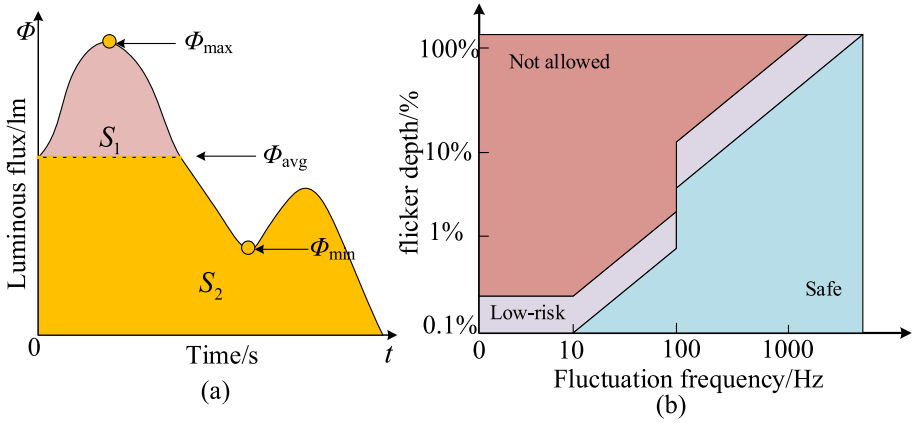

Fig. 6. Curves of (a) luminous flux over time and (b) flicker depth limit over frequency.

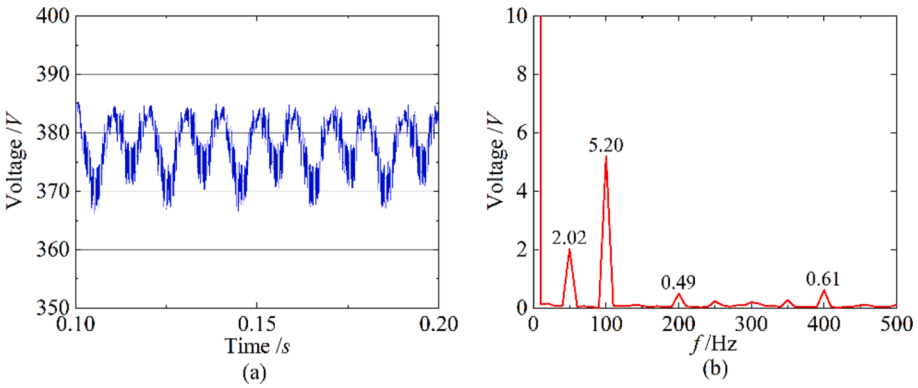

Fig. 8. The voltage waveform and Fourier analysis at the input side of the DC/AC converter.

while v_{dc} and i_{dc} denote the voltage and current on the DC side.

Assuming that the voltage of the single-phase AC load follows an ideal sinusoidal waveform, the voltage and current of the single-phase AC load can be expressed as:

$$\begin{cases} v_o = V_o \sin(\omega_o t) \\ i_o = I_o \sin(\omega_o t - \varphi) \end{cases} \tag{6}$$

Here, V_o and I_o are the amplitude of the single-phase AC load voltage and current, ω_o represents the angular frequency of the output voltage, and φ signifies the impedance angle of the single-phase AC load.

Based on the equations above, the instantaneous output power p_o of the DC/AC converter can be calculated as:

$$p_o = v_o i_o = \frac{1}{2} V_o I_o \cos\varphi - \frac{1}{2} V_o I_o \cos(2\omega_o t - \varphi) \tag{7}$$

From, it is evident that the instantaneous output power p_o of the DC/AC converter comprises two components: a DC component and an AC component with an angular frequency of $2\omega_o$. Assuming that the instantaneous input power p_{in} of the DC/AC converter is equal to the instantaneous output power p_o, the input current i_{in} of the DC/AC converter can be expressed as:

$$i_{in} = \frac{p_{in}}{V_{dc}} = \frac{V_o I_o}{2V_{dc}} \cos\varphi - \frac{V_o I_o}{2V_{dc}} \cos(2\omega_o t - \varphi) = I_{dc} + i_{2nd} \tag{8}$$

Consequently, the input current of the DC/AC converter also contains an AC component with an angular frequency of $2\omega_o$, which corresponds to the second harmonic component.

To validate the generation of second harmonic components by single-phase AC loads, a model as shown in Fig. 7 was constructed. The simulation results of the voltage and current at the input side of the DC/AC converter are displayed in Fig. 8. From the figure, it is evident that the input voltage at the inverter's input side, despite being nominally at 380 V, exhibits a noticeable superposition of the second harmonic component, consistent with theoretical analysis. In addition to the second harmonic component, there are also integer multiple harmonics of 50 Hz present.

3.4. DC voltage unbalance

In bipolar DC microgrid, the positive and negative voltages are not independent of each other. DGs power fluctuations, load imbalances, and asymmetric disturbances at the poles will cause unbalance average voltage, which can result in an unbalanced current on the neutral line and increase the loss of the feeder and grounding conductor. To assess the severity of positive and negative bus voltage imbalance in a bipolar DC microgrid, the concept of voltage unbalance coefficient needs to be defined. In [29], the voltage unbalance coefficient is expressed as:

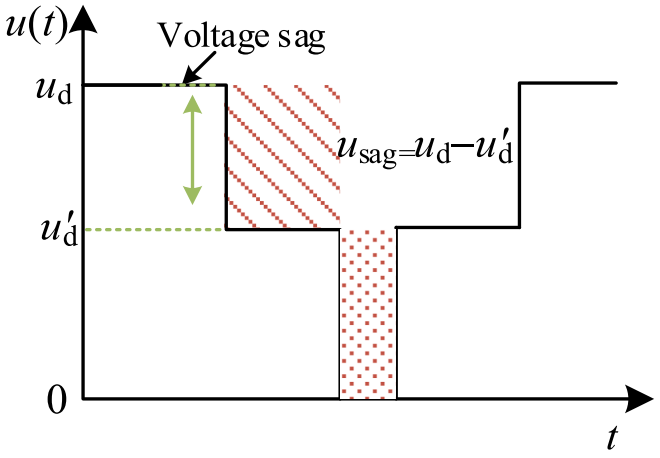

Fig. 9. Schematic diagram of voltage sag and interruption.

$$\varepsilon_u\% = \frac{|V_+ - V_-|}{0.5(V_+ + V_-)} \times 100\% \tag{9}$$

3.5. DC voltage deviation

Voltage deviation of DC microgrid is a basic index to measure the power quality. The voltage deviation is generally expressed as a percentage of the voltage deviation value to the nominal voltage of the system, and the expression is as follows:

$$\Delta U\% = \frac{U_i - U_{dN}}{U_{dN}} \tag{10}$$

Voltage deviation is mainly related to factors such as wire diameter, power supply distance, power flow distribution, and capacity, load power characteristics of electric energy transmission. The essence of voltage deviation is caused by the voltage drop generated on the internal resistance of the current flowing through the transmission network. Unlike the voltage drop generated by the AC power supply, the DC voltage drop is only related to conductor resistance [22].

3.6. DC voltage sag

Voltage sag is one of the typical power quality phenomena of the DC microgrids. DC buses short-circuit, micro-source power sudden change, DC load switching, and large power grid disturbance can cause DC voltage sag or interruption. The diagram of the DC voltage sag is shown in Fig. 9. It can be seen from Fig. 9 that the two most important features are the sag amplitude u_{sag} and the duration t_s. Different voltage levels

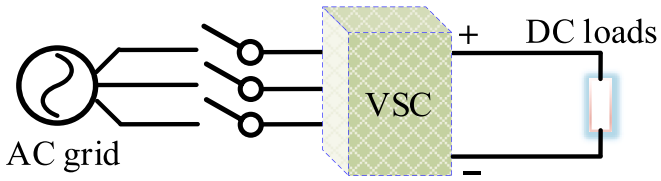

Fig. 10. Topology diagram for DC voltage harmonics analysis.

have different limitations on the sag duration and amplitude [55]. Compared with the AC grid, the loads in the DC microgrid are more sensitive to sudden voltage changes. Therefore, the requirements for voltage sags on the DC bus are more stringent. The sag depth $\Delta V_{sag}\%$ can be introduced to evaluate the severity of the voltage sag, and the expression is shown in Eq. (11),

$$\Delta V_{sag}\% = \frac{u_d - u_d'}{U_{dN}} \times 100\% = \frac{u_{sag}}{U_{dN}} \times 100\% \tag{11}$$

4. Correlation analysis and cases study

4.1. DC voltage harmonics analysis

Here, we take the harmonic characteristics of voltage source converters (VSC) as an example to analyze. The SPWM switching function of phase voltage is expanded by double Fourier serial, and the expansion includes three harmonic types:

1) Fundamental harmonic and fundamental band harmonic.
2) Carrier band harmonic: mf_c ($n = 0$, $m = 1,2,3,\cdots$).
3) Harmonics from carrier: $mf_c \pm nf_1$ ($m \neq 0$, $n \neq 0$). When there is a three-phase imbalance on the AC side of the VSC, the negative sequence component will cause an increase in the low-frequency component of the DC side. The low-frequency model of the switching function [5] is:

$$\begin{bmatrix} S_a \\ S_b \\ S_c \end{bmatrix} = M \begin{bmatrix} \cos(\omega t) \\ \cos(\omega t - \frac{2\pi}{3}) \\ \cos(\omega t + \frac{2\pi}{3}) \end{bmatrix} \tag{12}$$

Then the expression of the phase A current formed by each sequence component is:

$$i_a = I_{m1}\cos(\omega t - \varphi_1) + I_{m2}\cos(\omega t - \varphi_2) + I_{m0}\cos(\omega t - \varphi_0) \tag{13}$$

DC side current meets:

$$i_{dc} = \frac{S_a i_a + S_b i_b + S_c i_c}{2} = \frac{3}{4} M[I_{m1}\cos\varphi_1 + I_{m2}\cos(2\omega t - \varphi_1)] \tag{14}$$

It can be seen from Eq. (14) that: 1) the zero-sequence component of AC side current does not affect the harmonic distribution of the DC side current; 2) The instantaneous value of DC current is not only related to the amplitude of each sequence current but also related to their phase; 3) The negative sequence component of AC current is the main reason for the double frequency power fluctuation on the DC side.

The validation of the DC harmonic distribution rule is conducted utilizing the topology depicted in Fig. 10. The influence of harmonics in the bipolar DC grid is present in Fig. 11. The carrier ratio of PWM is set as 27 and the output of the PWM converter is served as the harmonic measurement point. Subsequently, the three-phase AC side voltage unbalance coefficient is set to 0 % and 2 %, respectively. The simulation results are shown in Fig. 12. When the three-phase voltage is balanced, the harmonics at the DC side are mainly the switching order and LCC harmonics. In addition, Fig. 12 presents that when the three-phase voltage is unbalanced, the harmonics on the DC side are mainly low-

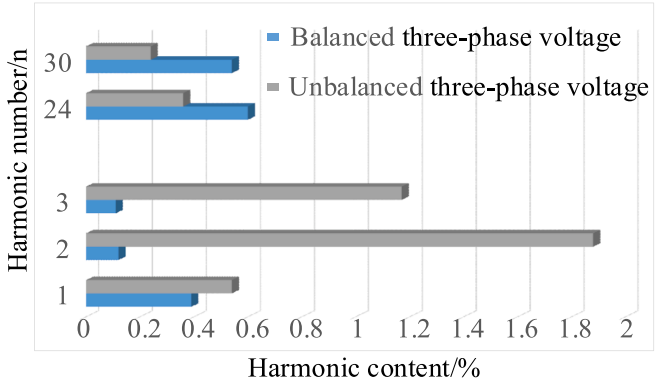

Fig. 12. DC side harmonic distribution under different conditions.

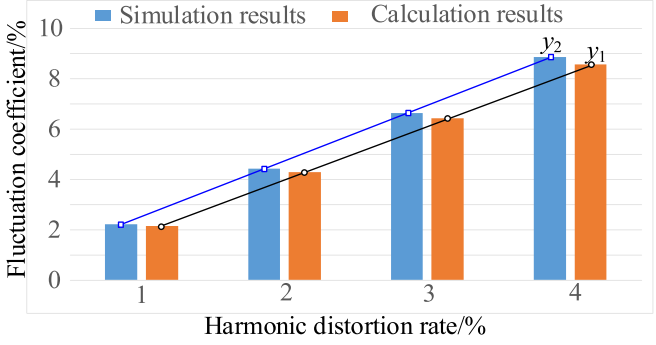

Fig. 13. Relationship between harmonic distortion rate and fluctuation coefficient.

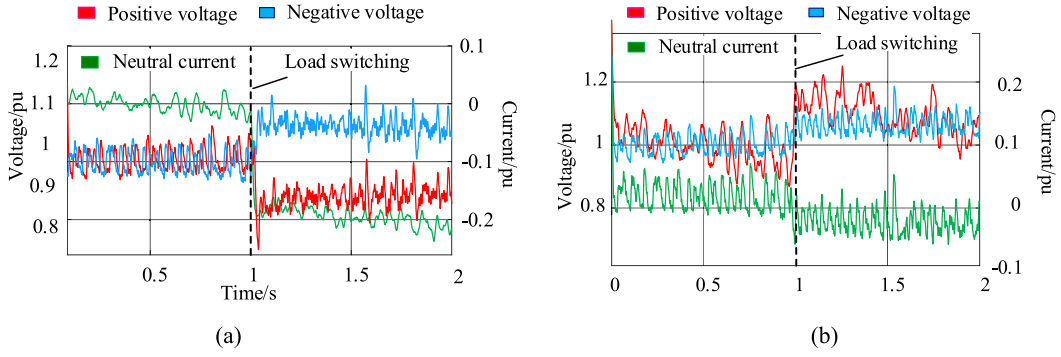

Fig. 11. Influence of harmonics in bipolar DC power network when switching the (a) positive load and (b) negative load.

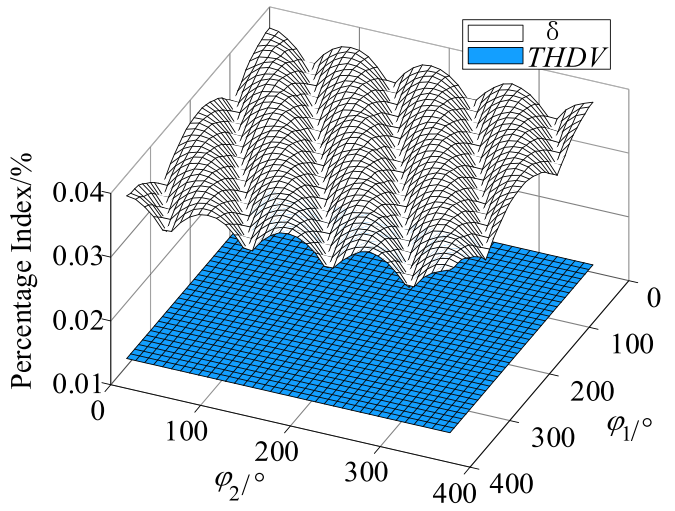

Fig. 14. Harmonic distortion rate and voltage fluctuation coefficient change with phase angle.

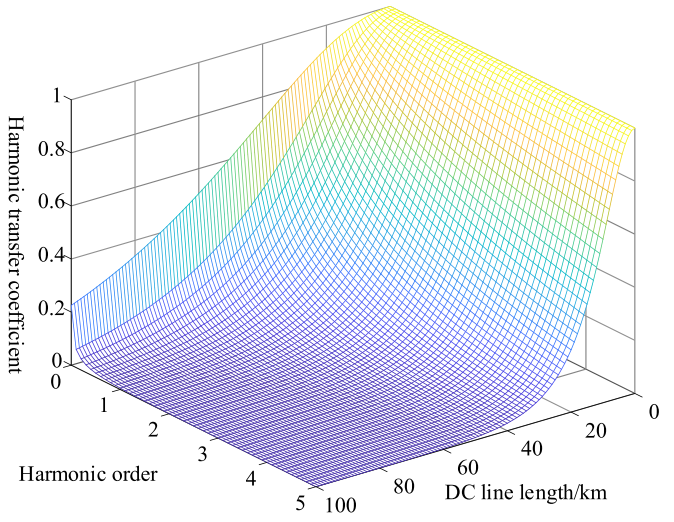

Fig. 15. Harmonic distortion rate and voltage fluctuation coefficient change with phase angle.

frequency harmonics, and the simulation results are consistent with the analysis.

By changing the voltage unbalance coefficient of three-phase voltage in the simulation model, the THD value of DC voltage is obtained by FFT tool. At the same time, the voltage fluctuation coefficient can be calculated according to Eq. (3). 10 groups of data are recorded to obtain the fitting curve y_1 of the relationship between harmonic distortion rate and fluctuation coefficient. It is assumed that the first harmonic content remains unchanged at 0.4 %, and the second harmonic content changes from 0.4 % to 4 %. 10 groups of harmonic distortion rate and fluctuation coefficient values are recorded to obtain the fitting curve y_2. Fig. 13 presents the fitting curves of y_1 and y_2. The harmonic distortion rate is approximately proportional to the voltage fluctuation coefficient and the simulation value is close to the calculated value in Fig. 13.

4.2. The correlation between harmonics and fluctuation

The harmonics on the DC side directly lead to the change of DC voltage amplitude, which can be regarded as the distortion of the DC voltage waveform and can be described by the change of the amplitude. For the DC voltage waveform, the instantaneous value u can be expressed as:

$$u = U_{d0} + \sqrt{2}U_1\sin(\omega t + \varphi_1) + \cdots + \sqrt{2}U_n\sin(n\omega t + \varphi_n) \quad = f(\boldsymbol{U}, \boldsymbol{\varphi}) \tag{15}$$

where $\boldsymbol{U} = [U_{d0}, U_1, U_2, \cdots, U_n]^T$; $\boldsymbol{\varphi} = [\varphi_1, \varphi_2, \cdots, \varphi_n]^T$; It can be seen from Eq. (15) that the instantaneous value of the DC side is a function of the RMS value of each harmonic and the initial phase angle. When $t \in (T, t + T)$, the voltage fluctuation coefficient can be expressed as:

$$\delta = \frac{\max f(\boldsymbol{U}, \boldsymbol{\varphi}) - \min f(\boldsymbol{U}, \boldsymbol{\varphi})}{U_{dN}} \tag{16}$$

Eqs. (15) and (16) present that the total harmonic distortion rate of voltage (*THDV*) is only related to the amplitude of the harmonic voltage. While δ is related to the initial phase angle of the harmonic. Setting the DC side only contains 1st and 2nd harmonics; U_1 and U_2 are 100 V and 50 V, respectively; $U_{d0} = U_{dN} = 400$ V, and the initial phase angle changes from 0° to 360°. According to Eq. (15), a three-dimensional curved surface of *THDV* and δ changing with phase angle can be obtained, as shown in Fig. 14. When the phase angle changes uniformly, the amplitude of δ changes periodically. It shows that the average value will fluctuate slightly, and the distribution of the maximum and minimum value meets a certain law. When the DC side contains 1st to n^{th} harmonics and the superposition of each harmonic has no obvious regularity,

The harmonic transfer coefficient between any two nodes in the DC microgrid is a function of harmonic order and line length, which is shown in Eq. (17). The transmission law of DC harmonics between two nodes can be obtained by substituting the line parameters in the DC microgrid, as shown in Fig. 15. With the increase of line length between nodes, the harmonic transfer coefficient has attenuation effect. Lower harmonics are easier to be transmitted than higher harmonics. Fig. 17.

$$\begin{cases} T_h = \cosh(\gamma_h l) - \dfrac{Z_{lh}}{Z_{Ch}}\sinh(\gamma_h l) \\ Z_{Ch} = \sqrt{z_{oh}/y_{oh}} \\ \gamma_h = \beta_h + j\alpha_h = \sqrt{z_{oh}y_{oh}} \\ Z_{lh} = Z_{Ch}\tanh(\gamma_h l) \end{cases} \tag{17}$$

4.3. Unbalanced voltage analysis

In order to further analyze the quantitative relationship between the bipolar unbalanced load and voltage unbalance coefficient, the equivalent model as shown in Fig. 16 is adopted. Then the positive and negative load voltages and voltage unbalance coefficient caused by the positive unbalanced loads are deduced. When resistance types are CRL and CPL respectively, the three-dimensional graphics of positive and negative load voltages, voltage sag depth, and voltage unbalance coefficient are similar. Therefore, this part only presents the three-dimensional diagram with the load type CPL.

According to, $\Delta V_{sag}\%$ for CRL and CPL are respectively shown in Eqs. (18) and (19), respectively:

$$\Delta V_{sag}\% = \frac{R_{Ld}}{R_L + R_{Ld}} - \frac{(R_{Ld} \| \Delta R)(3R_L + R_{Ld})}{2R_L(R_{Ld} \| \Delta R) + 2R_L R_{Ld} + (R_{Ld} \| \Delta R)R_{Ld} + 3R_L^2} \tag{18}$$

$$\Delta V_{sag}\% = \frac{\frac{R_{Ld}}{R_L + R_{Ld}}V_s - \frac{8(P_{Ld} + \Delta P)R_L}{-x_p + \sqrt{x_p^2 - 32R_L(P_{Ld} + \Delta P)}}}{V_s} \tag{19}$$

where $x_p = 3V_s - \sqrt{V_s^2 - 4R_L P_{Ld}}$. The three-dimensional graphics of the voltage unbalance coefficient and the positive sag depth varies with line resistance and CPL increment can be obtained from reference [56] and Eq. (19), as shown in Fig. 17.

In the simulation model shown in Fig. 16, the positive and negative poles are respectively connected to three groups of CRL. At the stage of 0 s-0.1 s, the positive and negative loads are balanced. Subsequently, the

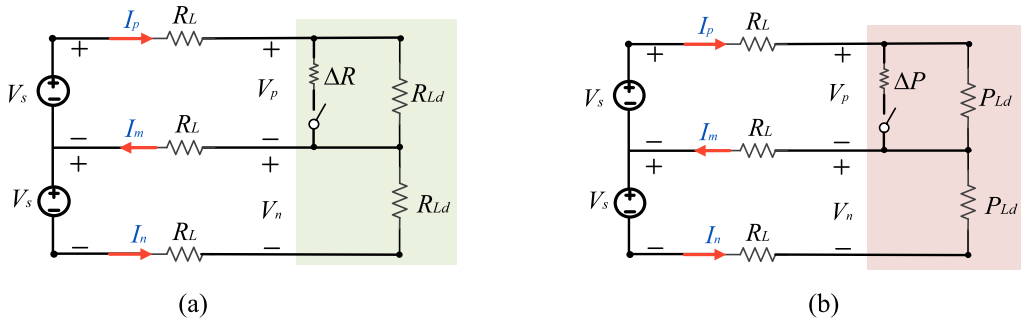

Fig. 16. The basic structure of the bipolar DC grid with (a) CRL and (b) CPL.

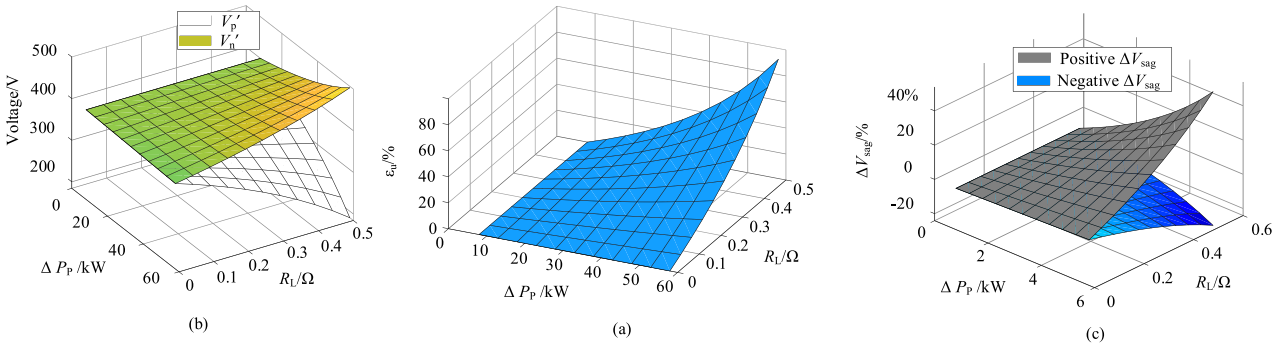

Fig. 17. The influence of line resistance and load increment on (a) positive and negative load voltage, (b) voltage unbalance coefficient, and (c) sag depth.

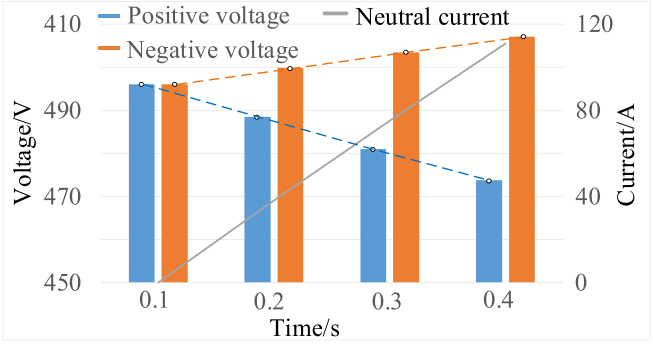

Fig. 18. Positive and negative voltages and neutral current changes with positive load input.

CRL is input at the positive every 0.1 s to measure the change of positive and negative voltage, as shown in Fig. 18. The voltage drop will be caused when the load is put into the positive pole. As the neutral current produces a voltage drop on the neutral line, the negative voltage will have a rise. It can be seen from the simulation results that every time the load is put on, the voltage drop of the positive pole is approximately 7.5 V, the voltage of the negative pole rises about 4 V, and the voltage unbalance coefficient is 2.3 %. The relationship between the positive voltage sag and the voltage unbalance coefficient is taken as an example, it is clear that the relationship is approximately proportional.

4.4. The correlation between transient unbalance and voltage sag

Increasing the allowable voltage deviation of the DC microgrid can increase the power supply radius and power supply range. However, allowing too much voltage deviation will increase the difficulty of converter design and control, and improve the requirements for equipment safety and insulation. Therefore, the voltage deviation of DC microgrid should be limited within a reasonable range. In the bipolar DC

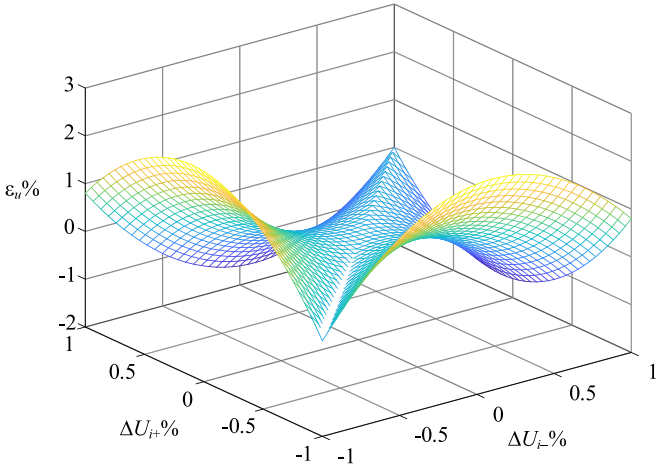

Fig. 19. The relationship between positive and negative voltage deviation and voltage unbalance.

microgrid, the correlation between DC voltage deviation and voltage imbalance needs to be considered, so the allowable range of DC voltage deviation needs to be reinvestigated.

According to the definition of voltage unbalanced coefficient and voltage deviation coefficient, the correlation between these two indicators is expressed as Eq. (20). When ΔU_{i+}% and ΔU_{i-}% vary from −1% to 1 %, the variations of ε_{ui}% is shown in Fig. 19. There is a significant correlation between voltage deviation and voltage unbalance.

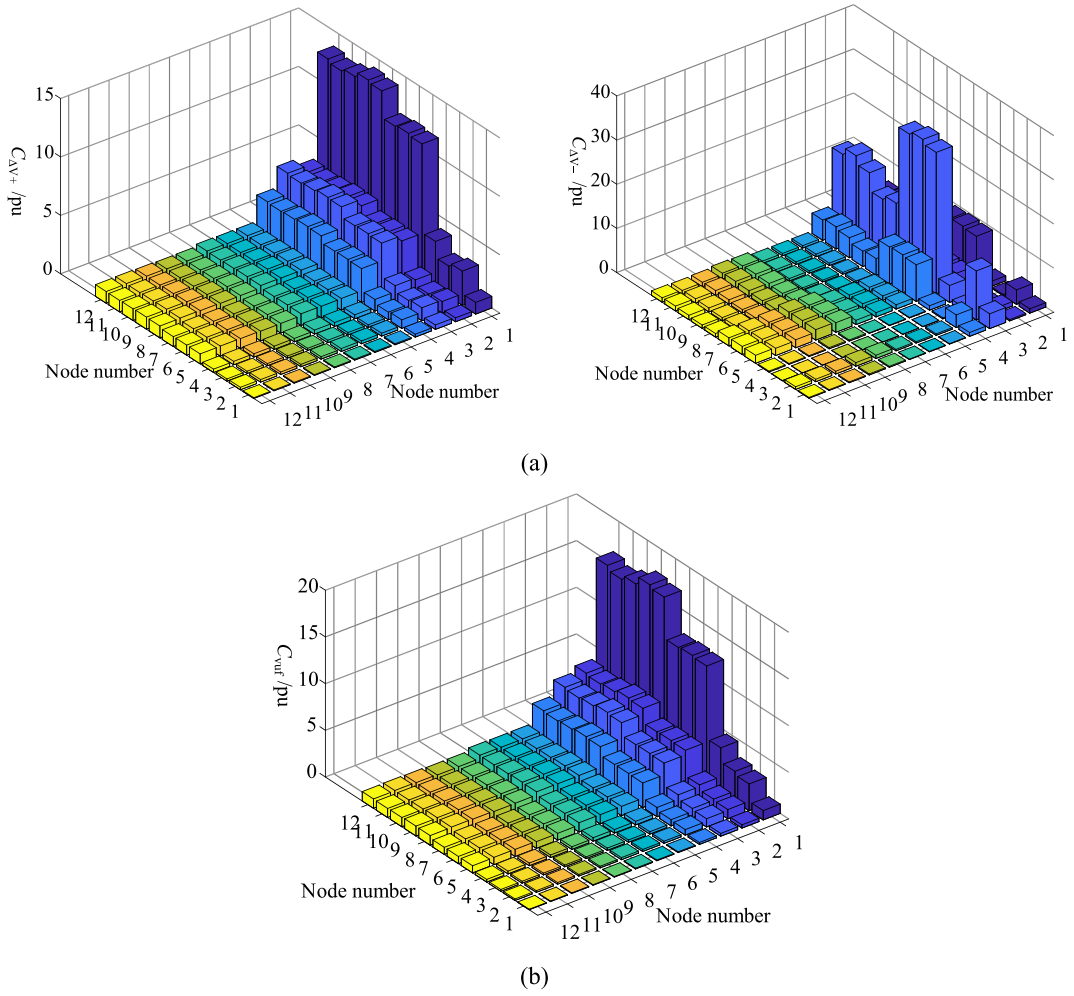

Fig. 20. Positive and negative voltages and neutral current changes with positive load input.

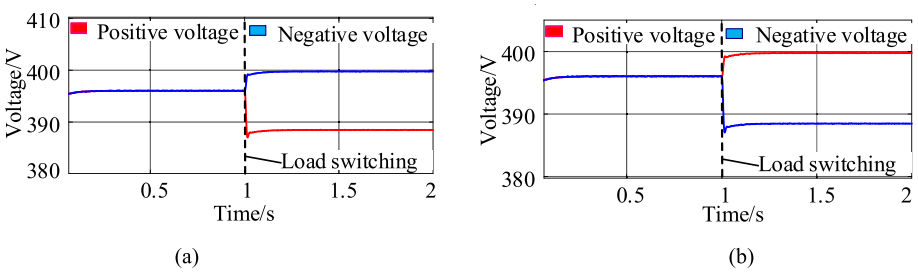

Fig. 21. Voltage sag and imbalance caused by the switching of the (a) positive load and (b) negative load.

$$\varepsilon_{ui}\% = \frac{|\Delta U_{i+}\% - \Delta U_{i-}\%|}{1+(\Delta U_{i+}\% + \Delta U_{i-}\%)} \times 100\% = \begin{cases} 1-\dfrac{1+2\Delta U_{i+}\%}{1+(\Delta U_{i+}\% + \Delta U_{i-}\%)}, & \Delta U_{i+}\% > \Delta U_{i-}\% \\ 0, & \Delta U_{i+}\% = \Delta U_{i-}\% \\ 1-\dfrac{1+\Delta U_{i-}\%}{1+(\Delta U_{i+}\% + \Delta U_{i-}\%)}, & \Delta U_{i+}\% < \Delta U_{i-}\% \end{cases} \tag{20}$$

In multiple nodes, the correlation between voltage deviation and voltage imbalance can be obtained by power flow calculation model. In this paper, the ratio of $\varepsilon_u\%$ and $\Delta U\%$ of nodes i and j are respectively defined as the correlation coefficient of unbalanced voltage and voltage deviation, so as to reflect the correlation between any two nodes in DC microgrid, as shown in Eq. (21).

The power flow calculation method in [57] is adopted to obtain the relations between voltage imbalance and voltage deviation in DC microgrid, as shown in Fig. 20. The load power at positive pole of node 1 changes and observe the voltage deviation and voltage imbalance of other nodes. As shown in Fig. 20, unbalanced voltage, and voltage deviation of $C_{\Delta V+}$ and C_{vuf} in multi-node DC microgrid has attenuation effect. However, the variation of $C_{\Delta V-}$ is related to the parameters of the network and the distribution characteristics of the load.

$$\begin{cases} C_{vuf} = \dfrac{\varepsilon_{ui}\%}{\varepsilon_{uj}\%} \\ C_{\Delta V+} = \dfrac{\Delta U_{i+}\%}{\Delta U_{j+}\%} \end{cases} C_{\Delta V-} = \frac{\Delta U_{i-}\%}{\Delta U_{j-}\%} \tag{21}$$

The simulation model of the bipolar DC microgrid is established with the negative fault and impact of positive load switching respectively, and the simulation results are shown in Fig. 21. The voltage and current in the figure are expressed in the unit values. It can be seen from Fig. 21 that under asymmetric disturbance, the positive and negative voltages are coupled with each other, and the voltage sag of one pole will cause voltage imbalance at the same time.

5. Conclusion

Combined with the existing literature and standards, this paper constructs the DC power quality index system and defines each DC power quality index, which can provide a reference for the subsequent formulation of relevant power quality standards. There are obvious correlations between voltage harmonic and fluctuation, voltage deviation and steady-state imbalance, voltage sag, and transient imbalance. It is an important basis for formulating DC power quality evaluation standards and index limits. This paper points out that according to the correlation between indexes, different power quality index sets can be selected for different applications to evaluate DC power quality. The paper also combines typical DC microgrid cases, derives the quantitative relationship between indicators and related parameters based on the definition of indicators, analyzes the generation mechanism of DC power quality, and verifies the correlation between power quality indicators.

This work was supported in part the National Natural Science Foundation of China (52207126), and the National Natural Science Foundation of China (52077017).

CRediT authorship contribution statement

Jianquan Liao: Conceptualization, Methodology, Writing – original draft, Writing – review & editing. **Chunsheng Guo:** Validation. **Xuefei Zhang:** Software. **Niancheng Zhou:** Project administration. **Qianggang Wang:** Supervision, Resources. **Wenfa Kang:** Project administration, Supervision, Resources, Writing – review & editing. **Juan C. Vasquez:** Writing – review & editing. **Josep M. Guerrero:** Writing – review & editing.

Declaration of competing interest

The authors declare that they have no known competing financial interests or personal relationships that could have appeared to influence the work reported in this paper.

Data availability

Data will be made available on request.

References

[1] van der Blij NH, Ramirez-Elizondo LM, Spaan MTJ, Bauer P. A State-Space Approach to Modelling DC Distribution Systems. IEEE Trans Power Syst 2018;33(1):943–50. https://doi.org/10.1109/TPWRS.2017.2691547.
[2] Wang R, et al. Simulation and power quality analysis of a Loose-Coupled bipolar DC microgrid in an office building. Appl Energy 2021;303:117606. https://doi.org/10.1016/j.apenergy.2021.117606.
[3] Lakshmi S, Ganguly S. An On-Line Operational Optimization Approach for Open Unified Power Quality Conditioner for Energy Loss Minimization of Distribution Networks. IEEE Trans Power Syst 2019;34(6):4784–95. https://doi.org/10.1109/TPWRS.2019.2919786.
[4] Li B, Liao K, Yang J, He Z. Transient Fault Analysis Method for VSC-Based DC Distribution Networks With Multi-DGs. IEEE Trans Ind Inf 2022;18(11):7628–38. https://doi.org/10.1109/TII.2022.3144149.
[5] Wang C, Li W, Wang Y, Meng Z, Yang L. DC Bus Voltage Fluctuation Classification and Restraint Methods Review for DC Microgrid. Proceedings of the CSEE 2017;37(1):84–97.
[6] Van den Broeck G, Stuyts J, Driesen J. A critical review of power quality standards and definitions applied to DC microgrids. Appl Energy 2018;229:281–8. https://doi.org/10.1016/j.apenergy.2018.07.058.
[7] Liao J, Zhou N, Wang Q. DC-side harmonic analysis and DC filter design in hybrid HVDC transmission systems. Int J Electr Power Energy Syst 2019;113:861–73. https://doi.org/10.1016/j.ijepes.2019.06.013.
[8] Khergade A, Satputaley R, Patro SK. Investigation of Voltage Sags Effects on ASD and Mitigation Using ESRF Theory-Based DVR. IEEE Trans Power Delivery 2021;36(6):3752–64. https://doi.org/10.1109/TPWRD.2020.3048838.
[9] Sun D, Long H, Zhou K, Lv Y, Zheng J, Chen Q. Research on SCESS-DFIG DC Bus Voltage Fluctuation Suppression Strategy for Frequency Inertia Regulation of Power Grid. IEEE Access 2020;8:173933–48. https://doi.org/10.1109/ACCESS.2020.3025292.
[10] Wang J, Xing Y, Wu H, Yang T. A Novel Dual-DC-Port Dynamic Voltage Restorer With Reduced-Rating Integrated DC–DC Converter for Wide-Range Voltage Sag Compensation. IEEE Trans Power Electron 2019;34(8):7437–49. https://doi.org/10.1109/TPEL.2018.2882534.
[11] Rolán A, Bogarra S, Bakkar M. Integration of Distributed Energy Resources to Unbalanced Grids Under Voltage Sags With Grid Code Compliance. IEEE Trans Smart Grid 2022;13(1):355–66. https://doi.org/10.1109/TSG.2021.3107984.
[12] "IEEE Guide for Analysis and Definition of DC Side Harmonic Performance of HVDC Transmision Systems." In: IEEE Std 1124-2003. 1-104. 5 Sept. 2003. doi: 10.1109/IEEESTD.2003.94382.
[13] Zhang L, Ruan X. Control Schemes for Reducing Second Harmonic Current in Two-Stage Single-Phase Converter: An Overview From DC-Bus Port-Impedance Characteristics. IEEE Trans Power Electron 2019;34(10):10341–58. https://doi.org/10.1109/TPEL.2019.2894647.
[14] Zhou W, Wu Y, Huang X, Lu R, Zhang H-T. A group sparse Bayesian learning algorithm for harmonic state estimation in power systems. Appl Energy 2021;306. https://doi.org/10.1016/j.apenergy.2021.118063.
[15] Liu G, Caldognetto T, Mattavelli P, Magnone P. Suppression of Second-Order Harmonic Current for Droop-Controlled Distributed Energy Resource Converters in DC Microgrids. IEEE Trans Ind Electron 2020;67(1):358–68. https://doi.org/10.1109/TIE.2019.2896071.
[16] You X, Liu H, Miao Y, Liao J, Huang Y. Stability Analysis and Active Damping Method of the Bipolar DC System with Constant Power Loads. Transactions of China Electrotechnical Society 2021:1–13. https://doi.org/10.19595/j.cnki.1000-6753.tces.201111.
[17] Li S, Lee ATL, Tan S, Hui SYR. Plug-and-Play Voltage Ripple Mitigator for DC Links in Hybrid AC–DC microgrids With Local Bus-Voltage Control. IEEE Trans Ind Electron 2018;65(1):687–98. https://doi.org/10.1109/TIE.2017.2708030.

[18] Xiao H. A Modular Low Current Ripple Electrolysis Power Supply Based on Multiphase Half-Bridge High-Frequency Inverters. IEEE Trans Power Electron 2020;35(10):10088–96. https://doi.org/10.1109/TPEL.2020.2978340.
[19] Zhao F, Xiao G, Zhao T. Accurate Steady-State Mathematical Models of Arm and Line Harmonic Characteristics for Modular Multilevel Converter. IEEE Trans Power Delivery 2018;33(3):1308–18. https://doi.org/10.1109/TPWRD.2017.2764950.
[20] Nejabatkhah F, Li YW, Tian H. Power Quality Control of Smart Hybrid AC/DC Microgrids: An Overview. IEEE Access 2019;7:52295–318. https://doi.org/10.1109/ACCESS.2019.2912376.
[21] Wang M, Yan S, Tan S, Hui SY. Hybrid-DC Electric Springs for DC Voltage Regulation and Harmonic Cancellation in DC Microgrids. IEEE Trans Power Electron 2018;33(2):1167–77. https://doi.org/10.1109/TPEL.2017.2681120.
[22] Zhang Y, Meng X, Shotorbani AM, Wang L. Minimization of AC-DC Grid Transmission Loss and DC Voltage Deviation Using Adaptive Droop Control and Improved AC-DC Power Flow Algorithm. IEEE Trans Power Syst 2021;36(1):744–56. https://doi.org/10.1109/TPWRS.2020.3020039.
[23] Wang M, Mok K, Tan S, Hui SY. Multifunctional DC Electric Springs for Improving Voltage Quality of DC Grids. IEEE Trans Smart Grid 2018;9(3):2248–58. https://doi.org/10.1109/TSG.2016.2609658.
[24] Jung T, Gwon G, Kim C, Han J, Oh Y, Noh C. Voltage Regulation Method for Voltage Drop Compensation and Unbalance Reduction in Bipolar Low-Voltage DC Distribution System. IEEE Trans Power Delivery 2018;33(1):141–9. https://doi.org/10.1109/TPWRD.2017.2694836.
[25] Guo C, Liao J, Zhang Y. Adaptive droop control of unbalanced voltage in the multi-node bipolar DC microgrid based on fuzzy control. Int J Electr Power Energy Syst 2022;142:108300. https://doi.org/10.1016/j.ijepes.2022.108300.
[26] C. Guo, Y. Wang, and J. Liao. "Coordinated Control of Voltage Balancers for the Regulation of Unbalanced Voltage in a Multi-Node Bipolar DC Distribution Network." *Electronics.* vol. 11, no. 1. 166. 2022. [Online]. Available: https://www.mdpi.com/2079-9292/11/1/166.
[27] Gu Y, Li W, He X. Analysis and Control of Bipolar LVDC Grid With DC Symmetrical Component Method. IEEE Trans Power Syst 2016;31(1):685–94. https://doi.org/10.1109/TPWRS.2015.2403310.
[28] Cui S, Lee J, Hu J, Doncker RWD, Sul S. A Modular Multilevel Converter with a Zigzag Transformer for Bipolar MVDC Distribution Systems. IEEE Trans Power Electron 2019;34(2):1038–43. https://doi.org/10.1109/TPEL.2018.2855082.
[29] He Z, et al. Optimized Modulation Method for Three-Level Boost Converter with ZVS Under Unbalanced-Load Operation. IEEE Trans Power Electron 2023;38(11):13811–24. https://doi.org/10.1109/TPEL.2023.3304300.
[30] S. Kan,X. Ruan, H. Dang, L. Zhang, andX. Huang. "Second harmonic current reduction in front-end dc–dc converter for two-stage single-phase photovoltaic grid-connected inverter." *IEEE Trans. Power Electron.* vol. 34, no. 7. 6399–6410. Jul. 2019.
[31] Pei Y, Tang Y, Xu H, Niu J, Ge L. A Modified Carrier-Based DPWM With Reduced Switching Loss and Current Distortion for Vienna Rectifier. IEEE Trans Power Electron 2023;38(10):12195–206. https://doi.org/10.1109/TPEL.2023.3298827.
[32] Li G, Ruan J, Wang K, Deng Y, He X, Wang Y. An Interleaved Three-Phase PWM Single-Stage Resonant Rectifier With High-Frequency Isolation. IEEE Trans Ind Electron 2020;67(8):6572–82. https://doi.org/10.1109/TIE.2019.2938461.
[33] "Electromagnetic compatibility (EMC) - Part 4-30: Testing and measurement techniques - Power quality measurement methods". In International Electrotechnical Commission, 2015.
[34] "IEEE Recommended Practice for Monitoring Electric Power Quality," in *IEEE Std 1159-2019 (Revision of IEEE Std 1159-2009)* , vol., no., pp.1-98, 13 Aug. 2019, doi: 10.1109/IEEESTD.2019.8796486.
[35] Han Y, Ning X, Yang P, Xu L. Review of Power Sharing, Voltage Restoration and Stabilization Techniques in Hierarchical Controlled DC Microgrids. IEEE Access 2019;7:149202–23. https://doi.org/10.1109/ACCESS.2019.2946706.
[36] Hannan MA, et al. Particle Swarm Optimization Algorithm Based Fuzzy Controller for Solid-State Transfer Switch Toward Fast Power Transfer and Power Quality Mitigation. IEEE Trans Ind Appl 2023;59(5):5570–9. https://doi.org/10.1109/TIA.2023.3289440.
[37] A. Saadat, R. -A. Hooshmand, A. Kiyoumarsi and M. Tadayon, "Optimal Location of Voltage Sag Monitors in Distribution Networks with DGs Using Network Zoning," in *IEEE Transactions on Power Delivery*, doi: 10.1109/TPWRD.2023.3302568.
[38] Badoni M, Singh A, Pandey S, Singh B. Fractional-Order Notch Filter for Grid-Connected Solar PV System With Power Quality Improvement. IEEE Trans Ind Electron 2022;69(1):429–39. https://doi.org/10.1109/TIE.2021.3051585.
[39] Liao J, Zhou N, Wang Q. Design of Low-Ripple and Fast-Response DC Filters in DC Microgrids. Energies 2018;11(11):pp.
[40] Alharbi MA, Dahidah MSA, Ali SA, Ethni SAE, Pickert V. Ripple-Free Multiphase Interleaved Stacked Converter for High-Power Applications. IEEE Trans Power Electron 2022;37(12):14770–80. https://doi.org/10.1109/TPEL.2022.3194979.
[41] Liao J, You X, Liu H, Huang Y. Voltage stability improvement of a bipolar DC system connected with constant power loads. Electr Pow Syst Res 2021;201:107508. https://doi.org/10.1016/j.epsr.2021.107508.
[42] Zhu X, Zhang Y, Jing S. A voltage ripple suppression method of DC microgrid under unbalanced load. Transactions of China Electrotechnical Society 2018;33(15):3437–49.
[43] Son G, Kim H-J, Cho B-H. Improved Modulated Carrier Control With On-Time Doubler for a Single-Phase Shunt Active Power Filter. IEEE Trans Power Electron 2018;33(2):1715–23. https://doi.org/10.1109/TPEL.2017.2682794.
[44] Ahrabi RR, Ding L, Li Y. Harmonics and Reactive Power Compensation of the LCC in a Parallel LCC-VSCs Configuration for a Hybrid AC/DC Network. IEEE Trans Energy Convers 2022;37(4):2913–25. https://doi.org/10.1109/TEC.2022.3198397.
[45] Xu Z, Kang D, Zhang R, Zhang J. Research on Harmonic Suppression Method of Series Six-Fold "Phase Hopping" AC-AC Frequency Converter. IEEE Trans Circuits Syst Express Briefs 2022;69(8):3480–4. https://doi.org/10.1109/TCSII.2022.3158939.
[46] L. Yang, A. Luo, Y. Chen, and et al. "The Second Harmonic Current Suppressed by Two Band-Pass Filters and Current Sharing Control Method of Bi-Directional Energy Storage Converters in DC Micro-grid." Proceedings of the CSEE. vol. 36, no. 6. 1613–1624.
[47] Kan S, Ruan X, Dang H, Zhang L, Huang X. Second Harmonic Current Reduction in Front-End DC−DC Converter for Two-Stage Single-Phase Photovoltaic Grid-Connected Inverter. IEEE Trans Power Electron 2019;34(7):6399–410. https://doi.org/10.1109/TPEL.2018.2877590.
[48] Wang T, et al. Energy Management Strategy Based on Optimal System Operation Loss for a Fuel Cell Hybrid Electric Vehicle. IEEE Trans Ind Electron 2024;71(3):2650–61. https://doi.org/10.1109/TIE.2023.3269477.
[49] Yang P, Xu S, Meng F, Zhang Z, Zhou R, Xu J. A Low Frequency Ripple Current Suppression Strategy for Single-Phase Photovoltaic Grid-Connected Inverter. IEEE J Emerging Sel Top Circuits Syst 2023;13(2):536–44. https://doi.org/10.1109/JETCAS.2023.3262768.
[50] Katir H, et al. Fault Tolerant Backstepping Control for Double-Stage Grid-Connected Photovoltaic Systems Using Cascaded H-Bridge Multilevel Inverters. IEEE Control Systems Letters 2022;6:1406–11. https://doi.org/10.1109/LCSYS.2021.3095107.
[51] Mahmud S, Collings W, Barchowsky A, Javaid AY, Khanna R. Global Maximum Power Point Tracking in Dynamic Partial Shading Conditions Using Ripple Correlation Control. IEEE Trans Ind Appl 2023;59(2):2030–40. https://doi.org/10.1109/TIA.2022.3228227.
[52] Nejabatkhah F, Li YW, Sun K, Zhang R. Active Power Oscillation Cancelation With Peak Current Sharing in Parallel Interfacing Converters Under Unbalanced Voltage. IEEE Trans Power Electron 2018;33(12):10200–14. https://doi.org/10.1109/TPEL.2018.2803770.
[53] Gerber DL, Ghatpande OA, Nazir M, Heredia WGB, Feng W, Brown RE. Energy and power quality measurement for electrical distribution in AC and DC microgrid buildings. Appl Energy 2021;308:118308. https://doi.org/10.1016/j.apenergy.2021.118308.
[54] Cai Y, Zou X, Gao Y, Li L, Mok PKT, Lau KM. Low-Flicker Lighting from High-Voltage LEDs Driven by a Single Converter-Free Driver. IEEE Photon Technol Lett 2017;29(19):1675–8. https://doi.org/10.1109/LPT.2017.2742861.
[55] Femine AD, Gallo D, Giordano D, Landi C, Luiso M, Signorino D. Power Quality Assessment in Railway Traction Supply Systems. IEEE Trans Instrum Meas 2020;69(5):2355–66. https://doi.org/10.1109/TIM.2020.2967162.
[56] Liao J, Zhou N, Huang Y, Wang Q. Unbalanced Voltage Analysis and Suppression Method in a Radial Bipolar DC Distribution Network. IEEE Journal of Emerging and Selected Topics in Power Electronics 2021;9(5):5687–702. https://doi.org/10.1109/JESTPE.2021.3068452.
[57] Chew BSH, Xu Y, Wu Q. Voltage Balancing for Bipolar DC Distribution Grids: A Power Flow Based Binary Integer Multi-Objective Optimization Approach. IEEE Trans Power Syst 2019;34(1):28–39. https://doi.org/10.1109/TPWRS.2018.2866817.